Journal of Hazardous Materials 482 (2025) 136485

Contents lists available at ScienceDirect

Journal of Hazardous Materials

journal homepage: www.elsevier.com/locate/jhazmat

# New insights into aqueous Hg(II) photoreduction from paddy field system to natural water: Gear effect of straw returning and soil tillage

Zhijun Fei [a], Zhuhong Wang [b,*], Jianxu Wang [c], Shouyang He [a,d], Qixin Wu [a,*], Pan Wu [a]

[a] Key Laboratory of Karst Georesources and Environment (Guizhou University), Ministry of Education, College of Resources and Environmental Engineering, Guizhou University, Guiyang 550025, China
[b] School of Public Health, The Key Laboratory of Environmental Pollution Monitoring and Disease Control, Ministry of Education, Guizhou Medical University, Guiyang 550025, China
[c] State Key Laboratory of Environmental Geochemistry, Institute of Geochemistry, Chinese Academy of Sciences, Guiyang 550082, China
[d] Guizhou Karst Environmental Ecosystems Observation and Research Station, Ministry of Education, Guiyang 550025, China

## HIGHLIGHTS

- Weak binding pool of Hg(II) decreased with depth, while strong binding pool increased.
- Solar radiation emerged as a limiting factor associated with high Hg/DOC ratio.
- Composition of SDOM dominated photoreduction at low Hg/DOC ratio.
- Gear effect of straw returning and soil tillage enhanced Hg(II) photoreduction.
- Gear effect reduced Hg burden in paddy system, but increased Hg(0) release flux.

## GRAPHICAL ABSTRACT

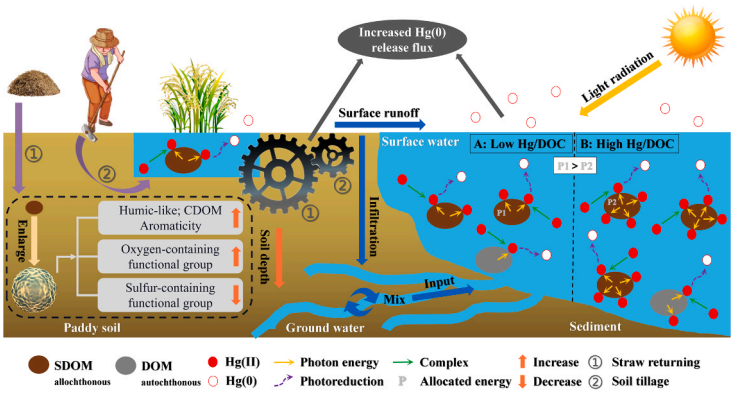


## ARTICLE INFO

*Keywords:*
Hg(II) photoreduction
SDOM
Straw returning
Soil tillage
Hg/DOC

## ABSTRACT

Soil dissolved organic matter (SDOM) has a strong complex with divalent mercury (Hg(II)) and can affect the fate of aqueous Hg(II) photoreduction. However, little is known about the influence of straw returning and soil tillage on the composition of SDOM in paddy soil and Hg(II) photoreduction in paddy water. Here, we demonstrate that the combined drivers of long-term straw returning and tillage can result in higher degrees of aromatization, and the enrichment of oxygen-containing functional groups in surface SDOM. Hg(II) photoreduction under low Hg/DOC conditions is mainly constrained by the composition of SDOM, whereas solar radiation emerged as a dominant controlling factor associated with high ratio of Hg/DOC. By increasing the release of SDOM and mobility of Hg(II), reducing the stability of Hg(II)-SDOM complexes, and potentially enhancing generation of reactive intermediates, gear effect of straw returning and soil tillage significantly enhanced Hg(II) photoreduction in the presence of surface SDOM from 0–40 cm (maximum photoreduction percentage can reach 44.76 ± 2.24 %). Previous inventories of Hg(0) emissions from paddy field system may have overlooked or

* Corresponding authors.
*E-mail addresses:* wangzhuhong@gmc.edu.cn (Z. Wang), qxwu@gzu.edu.cn (Q. Wu).

https://doi.org/10.1016/j.jhazmat.2024.136485
Received 10 August 2024; Received in revised form 3 November 2024; Accepted 9 November 2024
Available online 12 November 2024

underestimated this critical process. Future modeling work should be carried out to evaluate the role of straw returning and soil tillage on global Hg cycle.

## 1. Introduction

Mercury (Hg), a ubiquitously-distributed heavy metal pollutant, is of global environmental concern owing to its high volatility, long-distance migration, biomagnification, and toxicity to humans and biota [1,2]. Hg can be released into the environment via natural and anthropogenic activities, primarily existing as gaseous elemental mercury (GEM) [2]. Due to its prolonged residence time (~1 year) [3], GEM could be transported globally prior to deposition into terrestrial and aquatic ecosystems via atmospheric deposition [4]. In aquatic ecosystems, microbial activities convert a fraction of inorganic Hg to methylmercury (MeHg) [5], a potent neurotoxin that can accumulate up to $10^6$ times in the food chain compared to the surrounding environment [6,7]. Emission of gaseous Hg(0) from natural water bodies, due to aqueous Hg(II) photoreduction, decreases the possibility of Hg methylation but increases the fluxes of Hg(0) in the atmosphere [8,9]. Understanding the mechanism and dynamics of Hg(II) photoreduction in natural water is crucial for gaining insights into the global Hg cycle.

The fate of aqueous Hg(II) photoreduction can be influenced by dissolved organic matter (DOM) [8,10–14]. As a crucial ligand for Hg (II), DOM has a significant impact on the photochemical transformation of Hg(II) [15]. Although inorganic Hg, like $Hg(OH)_2$, can be photo-reduced at very slow rates, the formation of Hg-DOM complex is a prerequisite for Hg(II) photoreduction [16,17]. Early modeling work suggested that 94–99 % of dissolved Hg(II) in natural water was complexed with DOM [18]. Field studies inform that photoreduction of Hg-DOM complexes could result in large Hg(0) outflux at the water-air interface [8,12,19]. However, experimental studies have not reached a consistent conclusion on the role of DOM in Hg(II) photoreduction. Some studies demonstrated a notable increase in Hg(II) photoreduction under high DOM conditions [9,10,15,20,21]. A few studies, however, have shown that high concentration of DOM is detrimental to Hg(II) photoreduction [13,22–24]. Overall, the role of DOM in aqueous Hg(II) photoreduction remains poorly understood.

Paddy fields, as a unique wetland ecosystem, are widely distributed globally. The amount of straw produced annually by rice cultivation is enormous [25]. As a green and environmentally friendly straw treatment method, long-term straw returning not only increases grain yields and soil organic matter (SOM) storage but also alters the composition of Soil-DOM (SDOM) [26,27]. Simultaneously, soil tillage, as a beneficial practice after straw returning and prior to rice cultivation, exacerbates the loss of SOM pool and changes the composition of SDOM to a certain extent [28,29]. SDOM is an indispensable source of DOM in aquatic ecosystem [30], and plays a crucial role in forming organometallic complexes [31]. Studies have focused on the effect of SDOM on Hg methylation and enrichment within paddy systems [32–36]. However, precious little attention has been paid to the impact of paddy SDOM on aqueous Hg(II) photoreduction, and little is known about vertical differences in SDOM composition within the same paddy soil profile under the combined effects of long-term straw returning and soil tillage. As paddy fields are hotspots of the Hg biogeochemical cycle [36,37], it is crucial to evaluate the role of paddy SDOM on Hg(II) photoreduction.

Here we collected layered paddy soil affected by years of straw returning and tillage, and conducted field and laboratory experiments to (1) characterize and analyse the differences in layered SDOM composition; (2) establish the dynamics of Hg(II) photoreduction in SDOM-containing waters, and (3) evaluate the role of SDOM on aqueous Hg (II) photoreduction and Hg(0) release flux. This study helps to re-examine the impact of SDOM, affected by two common measures for farmland management (straw returning and soil tillage), on Hg(II) photoreduction, as well as to ascertain whether the contribution of this process to Hg(0) emission inventories has been underestimated or overlooked for a long time.

## 2. Materials and methods

### 2.1. Materials

A paddy field (32 $m^2$: 8 m × 4 m), as the sampling area for experimental soil, was selected (26°30′16.23′ N, 106°26′20.48′ E) near Hongfeng Lake, Guizhou Province, SW China (Fig. 1). Through visiting and investigational study and four years of continuous on-site follow-up from 2019 to 2023, it was confirmed that the sampled filed had been implementing straw returning and soil tillage for more than 8 consecutive years. During the non-flooded period, paddy soil samples were obtained from different intervals of a soil profile (Depth: 0–20 cm, 20–40 cm, 40–60 cm, 60–80 cm and 80–100 cm; 20 kg for each interval). The samples were preserved in clean sealed bags and promptly transported into the laboratory. The samples were air-dried, crushed, sieved to 10-mesh, and homogenized, prior to being used for the soil tillage and leaching experiment.

### 2.2. Extraction of SDOM

A portion of soil was ground and sieved to 100-mesh, and stored in light-proof clean sealed bags for subsequent physicochemical analysis. The soil sample was also mixed with water at a ratio of 1 g:10 mL (v/m) and thoroughly shaken [30], and then incubated at a constant temperature of 25 °C in the dark with shaking at 200 r $min^{-1}$ for 24 h, followed by centrifugation at 4000 r $m^{-1}$ for 30 min. The supernatant was filtered through 0.45 μm cellulose-acetate membrane (Whatman, England) to obtain the SDOM solution, which was then freeze-dried (FDU-1110, Eyela, Japan). The obtained solid SDOM samples from different soil intervals were used for structural and compositional analysis.

### 2.3. Soil tillage and leaching experiment

#### 2.3.1. Soil tillage experiment

Customized containers were used for the soil tillage experiment (Fig. S1). Briefly, 2000 $cm^3$ of soil powder was placed into a PVC rectangular container (length: 20 cm, width: 10 cm; height: 20 cm). Each soil interval was equipped with the control group (CG) and the tillage group (TG) (set up three parallel groups for each group). Each group was added with an appropriate amount of Milli-Q water and aged for 3 days, then adjusted to 70 % of maximum field capacity with Milli-Q Water. All groups were placed outdoors, with a layer of transparent film positioned 20 cm above each group to minimize dust and other contaminants. The control group received no treatment, while the experimental group was evenly tilled once. After 7 days, a 20 mL subsample of the solution was taken from each group and filtered through 0.45 μm cellulose-acetate membrane. All samples were preserved in a refrigerator at 4 ℃ before testing.

#### 2.3.2. Soil leaching experiment

A device was designed for soil leaching (Fig. S2). Briefly, ~ 2.50 kg of soil powder was placed into a PVC column (internal diameter: 5 cm; height: 20 cm). The column was leached by Milli-Q water at a consistent rate (60 mL $Day^{-1}$) for 30 days. Eventually, about 5.10 L of leachate was collected from each soil interval. Soil leachates were filtered through 0.45 μm cellulose-acetate membrane and preserved in a refrigerator at 4 ℃ before the photoreduction experiment.

### 2.4. Hg(II) photoreduction experiment

Hg(II) photoreduction experiment was conducted by adding 400 mL of soil leachate into 2 L Griffin beakers. Variable masses of Hg, derived from a concentrated Hg standard solution (NIST-3133, 100 ppm Hg), were then added into 20 beakers, yielding varying Hg concentrations (2 ng $mL^{-1}$, 5 ng $mL^{-1}$, 10 ng $mL^{-1}$ and 20 ng $mL^{-1}$) and variable Hg/DOC values for the leachates contained (Table 1). Three parallel groups were set up for each Hg/DOC ratio at the same depth (e.g., three identical experimental groups were set up for B1). The beakers were placed in an open field and exposed to sunlight for 72 h (Fig. S3). One subsample (3.50 mL each) was sampled from each beaker at different time intervals (Day1: 8 am, 9 am, 10 am, 12 am, 2 pm, 6 pm; Day 2: 6 am, 12 am, 6 pm; Day 3: 6 am, 12 am, 6 pm), and were preserved in 20 mL pre-cleaned high borosilicate glass bottles, which contained 0.5 % BrCl and were stored in dark conditions to prevent Hg reduction. Overall, a total of 720 sub-samples were collected. During this experiment, no rainfall or other adverse weather events occurred. Solar radiation data was obtained from the Meteorological Bureau of Guizhou Province (Fig. S4).

### 2.5. Sample analysis

#### 2.5.1. Determination of Hg and DOC concentration

The THg content of the paddy soil sample was determined with a DMA-80 Hg analyzer (Milestone, Italy). Hg concentration of subsamples was measured by cold vapor atomic fluorescence (CVAFS) (Model III, Brooksrand, USA). DOC values of the leachates and TOC values of soil were measured by using a TOC analyzer (vario TOC cube, Elementar, Germany). Based on in-situ analyses by a pH meter (ST3100/F, Ohaus, USA), the pH values of paddy soil and leachates were determined.

#### 2.5.2. Characterization analysis of SDOM

UV-Vis and fluorescence measurements for SDOM were performed using a simultaneous absorption-3D fluorescence spectrometer (Aqualog-UV-800C, Horiba, Japan). The surface morphology of freeze-dried SDOM samples was examined by scanning electron microscopy (SEM: Apreo 2C, Thermo Scientific, USA). In addition, the chemical composition and structural information of freeze-dried SDOM samples were identified by Fourier transformation infrared spectroscopy (FTIR: IRTracer-100, Shimadzu, Japan) and X-ray photoelectron spectroscopy (XPS: EscaLab Xi+, Thermo Fisher Scientific, USA). Detailed information on measurements and related data analysis are described in the Supplementary Material. The calculation and description of spectral parameters are shown in Table S2.

**Table 1**
Initial Hg and DOC concentration, and Hg/DOC ratios for Hg(II) photoreduction experiment. B1-B20: The letter B stands for the abbreviation of beaker, while the digit represent the serial number.

| Beaker number | Sample depth (cm) | DOC (mg $L^{-1}$) | Exogenous Hg (ng $mL^{-1}$) | Hg/DOC (ng $mg^{-1}$) | Light source |
|---|---|---|---|---|---|
| B1 | 0–20 | 85.83 | 2 | 23 | Natural sunlight |
| B2 | | | 5 | 58 | |
| B3 | | | 10 | 117 | |
| B4 | | | 20 | 233 | |
| B5 | 20–40 | 37.85 | 2 | 53 | |
| B6 | | | 5 | 132 | |
| B7 | | | 10 | 264 | |
| B8 | | | 20 | 528 | |
| B9 | 40–60 | 30.11 | 2 | 66 | |
| B10 | | | 5 | 166 | |
| B11 | | | 10 | 332 | |
| B12 | | | 20 | 664 | |
| B13 | 60–80 | 26.06 | 2 | 77 | |
| B14 | | | 5 | 192 | |
| B15 | | | 10 | 384 | |
| B16 | | | 20 | 767 | |
| B17 | 80–100 | 18.77 | 2 | 107 | |
| B18 | | | 5 | 266 | |
| B19 | | | 10 | 533 | |
| B20 | | | 20 | 1066 | |

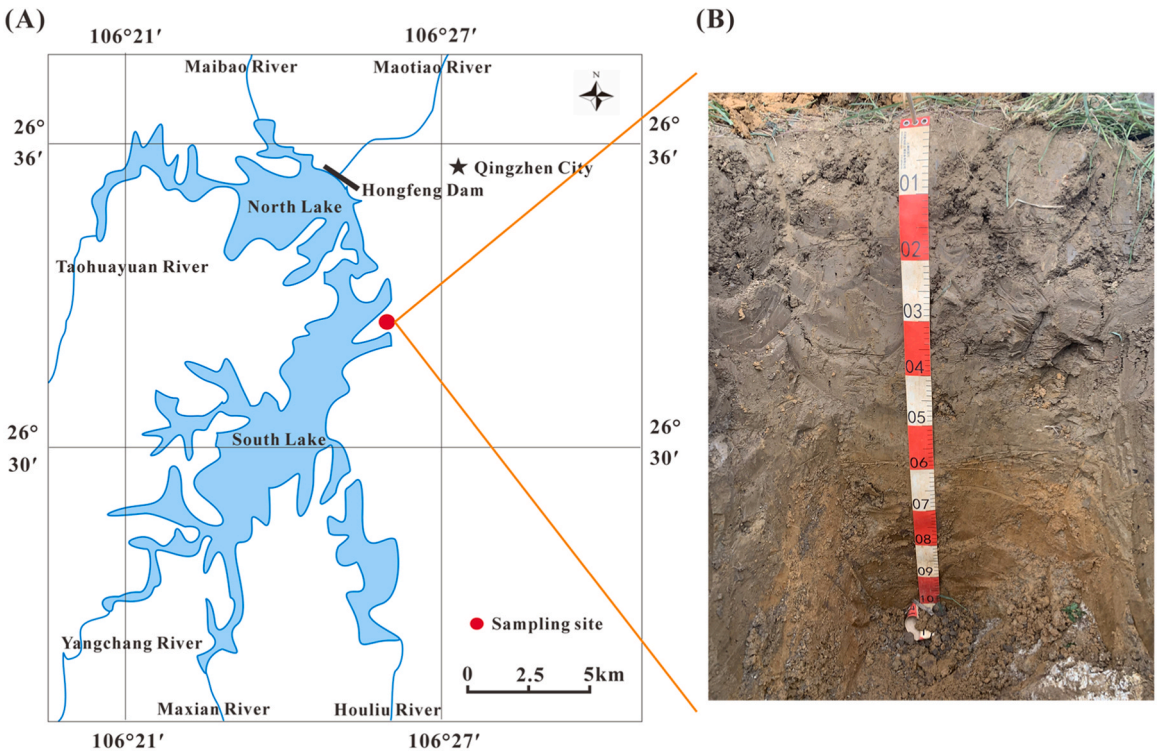


**Fig. 1.** (A) Locations of paddy soil sampling site; (B) On site sampling of soil profile map.

### 2.5.3. Quality assurance and quality control

Quality assurance and quality control for the THg analyses were conducted using duplicates, matrix spikes and/or standard reference materials. Measurement of soil reference material (GBW07405, IGGE, China) yielded Hg recoveries of 90–110 %. Measurement of Hg spiked solutions (NIST-3133, 100 ppm Hg), yielded Hg recoveries of 90–110 % as well. All duplicate samples' relative standard deviations were below 10 %.

## 3. Results

### 3.1. Vertical distribution of TOC/DOC and THg concentrations

TOC concentrations in paddy soil profile showed a decreasing pattern from top to deep layers (0.47 mg $g^{-1}$, 0.31 mg $g^{-1}$, 0.12 mg $g^{-1}$, 0.11 mg $g^{-1}$, and 0.09 mg $g^{-1}$, respectively). Gradual declining variation of DOC levels in paddy soil leachates was also observed, with 85.83 mg $L^{-1}$, 37.85 mg $L^{-1}$, 30.11 mg $L^{-1}$, 26.06 mg $L^{-1}$, and 18.77 mg $L^{-1}$, separately (Table S1 and Fig. S5-A). THg concentrations, ranging from 69.93 to 197.87 ng $g^{-1}$ in paddy soil samples and 2.66 to 11.23 ng $L^{-1}$ in soil leachates, also displayed a decreasing pattern from

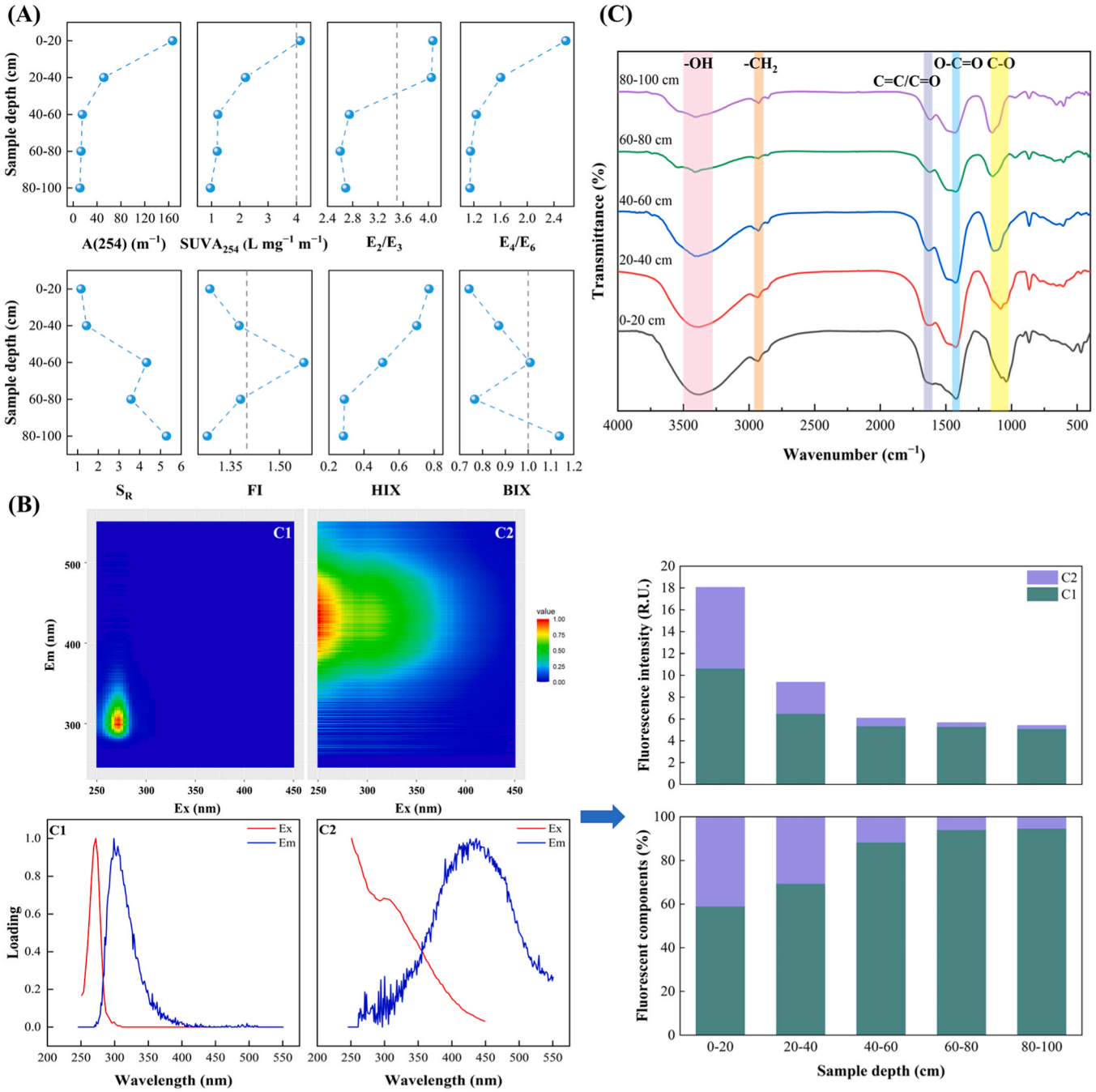


**Fig. 2.** (A) Optical indices of SDOM from different paddy soil intervals. A(254), $SUVA_{254}$, $E_2/E_3$, $E_4/E_6$ and $S_R$ represent the characteristics of UV-Vis spectrum, while FI, HIX and BIX represent the characteristics of fluorescence spectrum. The grey dashed line represents the criteria value of index; (B) Two fluorescent components for SDOM from different paddy soil intervals. C1 represents tryptophan-like component, while C2 represents fulvic acid-like component; (C) FTIR of SDOM from different paddy soil intervals.

top to deep layers. Positive correlations were observed between TOC and THg concentration in paddy soil samples ($r = 0.97$, $p < 0.01$), while there was no significant correlation between DOC and THg concentration in soil leachates ($r = 0.85$, $p > 0.05$) (Table S1 and Fig. S5-B, C).

### 3.2. Vertical differences in SDOM composition

#### 3.2.1. Characteristics and properties of SDOM

*3.2.1.1. UV–Vis and 3D-EEM analysis.* A(254) value (51.53–166.65 $m^{-1}$) of surface SDOM from 0–20 cm and 20–40 cm (termed as $SDOM_{0–20,20–40}$) was significantly higher than that of deep SDOM from 40–60 cm, 60–80 cm and 80–100 cm (termed as $SDOM_{40–60,60–80,80–100}$) (11.56–15.45 $m^{-1}$) (Fig. 2-A), with the highest A(254) value in SDOM from 0–20 cm (termed as $SDOM_{0–20}$), indicating that $SDOM_{0–20,20–40}$ contained a large amount of unsaturated structural substances and had a higher concentration of chromophoric dissolved organic matter (CDOM) [38]. $SUVA_{254}$ value decreased continuously with increasing depth (0.96–4.14 L $mg^{-1}$ $m^{-1}$). Notably, the difference in $SDOM_{40–60,60–80,80–100}$ is minimal (0.96–1.23 L $mg^{-1}$ $m^{-1}$), and only $SDOM_{0–20}$ has a $SUVA_{254}$ value greater than 4 L $mg^{-1}$ $m^{-1}$, informing the presence of more aromatic substances, higher degrees of aromatization and a relatively advanced state of humification in $SDOM_{0–20,20–40}$ [39]. Additionally, $E_2/E_3$ value of $SDOM_{0–20,20–40}$ was greater than 4, indicating a higher fulvic acid (FA) content than humic acid (HA) content. In contrast, $E_2/E_3$ value of $SDOM_{40–60,60–80,80–100}$ ranged from 2.60 to 2.75, suggesting a lower level of FA than that of HA [40]. $E_4/E_6$ value of $SDOM_{0–20}$ was the highest and decreased with increasing depth, informing the degree of polymerization of benzene ring carbon (C) skeleton increased with depth [41]. $S_R$ value is inversely proportional to molecular weight of DOM [42]. In this study, the molecular weight of $SDOM_{0–20,20–40}$ was larger than that of $SDOM_{40–60,60–80,80–100}$, which was consistent with the implication of $SUVA_{254}$ value.

Fluorescence index (FI) and biological index (BIX) are both used to characterize the source of DOM [43,44]. In this study, apart from SDOM from 40–60 cm ($1.40 < FI = 1.58 < 1.90$), FI of SDOM from other soil intervals were all below 1.40 (FI: 1.28–1.38), indicating primarily allochthonous input [43]. Meanwhile, BIX of $SDOM_{0–20,20–40}$ was less than 1 (BIX: 0.74–0.87), indicating a relatively minor contribution from autochthonous source [44]. The humification index (HIX) of different soil intervals decreased with depth, suggesting that $SDOM_{0–20,20–40}$ (HIX: 0.70–0.77) had a relatively higher degree of humification compared to $SDOM_{40–60,60–80,80–100}$ (HIX: 0.28–0.51) [44].

There were two distinct fluorescence peak regions in the SDOM from different soil intervals (Fig. 2-B), identified as the tryptophan-like (protein-like: C1) and the fulvic acid-like (humus-like: C2) (Table S3). For $SDOM_{0–20,20–40}$, the proportion of C1 component was the lowest, while that of C2 component was the highest. The proportion of C1 component in SDOM increased whereas that of C2 component decreased with depth. Therefore, $SDOM_{0–20,20–40}$ primarily originated from allochthonous input, containing more humic-like components, larger molecular weight and higher degrees of humification and aromatization. Notably, the fluorescence index of $SDOM_{0–20}$ differed significantly from that of SDOM from other soil intervals.

*3.2.1.2. FTIR analysis.* FTIR spectra of SDOM from different paddy soil intervals were shown in Fig. 2-C. Oxygen-containing functional groups were mainly observed. Compared to $SDOM_{40–60,60–80,80–100}$, $SDOM_{0–20,20–40}$ exhibited a larger and broader absorption peak in the wavelength range of 3300–3500 $cm^{-1}$, which can be attributed to -OH (hydroxyl group) stretching vibration [45]. The bands at around 2930 $cm^{-1}$ were assigned to C-$H_2$ asymmetric vibration of aliphatic groups, while the bands at 1650–1600 $cm^{-1}$ were assigned to C═C (aromatic group) or C═O (carbonyl group) [46]. The vibrational intensities of peaks at 1440–1420 $cm^{-1}$ and 1150–1000 $cm^{-1}$ were O-C═O (carboxyl group) asymmetric stretching vibration and C-O stretching of alcohols, ethers, and carbohydrates [47,48], respectively. The peak areas corresponding to O-C═O and C-O in $SDOM_{0–20,20–40}$ were relatively larger, indicating a higher content of carboxyl groups. Therefore, SDOM from different paddy soil intervals contained oxygen-containing functional groups such as hydroxyl and carboxyl groups, and the content of these groups was relatively higher in $SDOM_{0–20,20–40}$.

*3.2.1.3. XPS analysis.* According to the C 1s and O 1s spectrum (Fig. 3-A), the content of C-O-H (hydroxyl group), O-C═O (carboxyl group) and C═O (carbonyl group) in SDOM from different paddy soil intervals decreased sequentially with depth (C-O-H: 25.72–53.43 %; O-C═O: 8.52–15.21 %; C═O: 8.89–12.46 %). In comparison with $SDOM_{40–60,60–80,80–100}$, $SDOM_{0–20,20–40}$ contained relatively higher contents of C-O-H, O-C═O and C═O. Surface sulfur (S) content of SDOM from different paddy soil intervals increased gradually with depth (S: 0–2.15 %). Conversely, surface nitrogen (N) and oxygen (O) decreased sequentially with depth (N: 0–2.65 %; O: 36.06–41.07 %) (Fig. S6). This indicated that, compared to $SDOM_{40–60,60–80,80–100}$, $SDOM_{0–20,20–40}$ had an extremely lower content of sulfur-containing functional groups, while nitrogen- and oxygen-containing functional groups were relatively higher.

#### 3.2.2. Surface morphology of SDOM

Significant differences in appearance and color were observed among SDOM solid samples (Fig. S7). Specifically, $SDOM_{0–20,20–40}$ predominantly exhibited light brown, appearing as aggregated floccules. $SDOM_{40–60,60–80,80–100}$ were mainly off-white and displayed dispersed floccules. At the micro- (μm) and nanometer- (nm) scales, surface of $SDOM_{0–20,20–40}$ was predominantly composed of stacked or interconnected spheres of varying sizes (Fig. 3-B). These spheres showed relatively smooth surface and the overall structure is loose. For $SDOM_{40–60,60–80,80–100}$, surface morphology underwent notable alteration, exhibiting a sheet-like or layered distribution. The surface was relatively rough and adorned with numerous granular protrusions. Furthermore, as the depth increased, the overall pore and crack structures became more pronounced and well-developed.

After years of straw returning and soil tillage to the paddy field system, $SDOM_{0–20,20–40}$ exhibited increased molecular weight and enhanced aromaticity. Concurrently, $SDOM_{0–20,20–40}$ was enriched with oxygen-containing functional groups, including hydroxyl, carboxyl and carbonyl groups, as well as nitrogen-containing functional groups, while sulfur-containing functional groups were present in exceedingly low levels. This suggested that the long-term practice of straw returning and tillage had contributed to the accumulation of structurally complex and chemically active SDOM in the surface paddy soil (0–20 cm and 20–40 cm).

### 3.3. Differences in DOC release levels during tillage

For CG, as soil depth increased, DOC concentration levels released from different paddy soil intervals were 36.55 ± 1.67 mg $L^{-1}$, 17.22 ± 0.27 mg $L^{-1}$, 4.86 ± 0.22 mg $L^{-1}$, 4.04 ± 0.25 mg $L^{-1}$ and 4.13 ± 0.69 mg $L^{-1}$, respectively (Fig. 4). While DOC concentration levels for TG were 58.16 ± 1.46 mg $L^{-1}$, 26.79 ± 0.16 mg $L^{-1}$, 7.36 ± 0.16 mg $L^{-1}$, 6.53 ± 0.43 mg $L^{-1}$ and 6.14 ± 0.18 mg $L^{-1}$, separately. Compared to CG, DOC concentrations for TG increased significantly by 59.14 %, 55.57 %, 51.45 %, 61.67 % and 48.78 %, respectively. Additionally, in both CG and TG, DOC levels released from surface soil (0–20 cm and 20–40 cm) were significantly higher than those in deep soil (40–60 cm, 60–80 cm and 80–100 cm), exceeding over 3.5 times. Given that the depth of soil tillage within paddy field system was typically limited to 0–40 cm [29,49], it indicated that soil tillage could substantially enhance the release of $SDOM_{0–20,20–40}$,

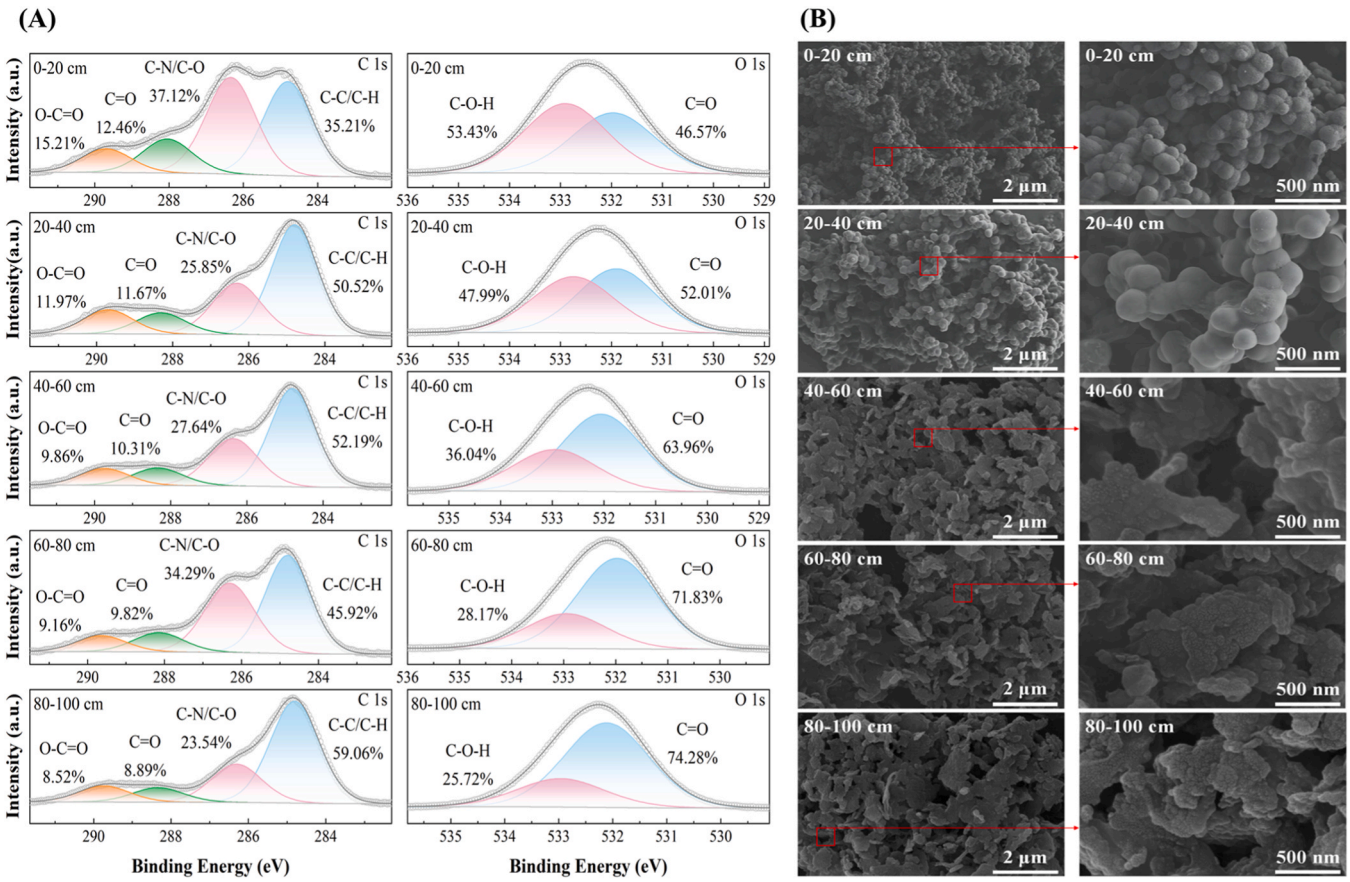


**Fig. 3.** (A) XPS of SDOM from different paddy soil intervals; (B) SEM of SDOM from different paddy soil intervals at the micro- (2 μm) and nanometer- (500 nm) scales.

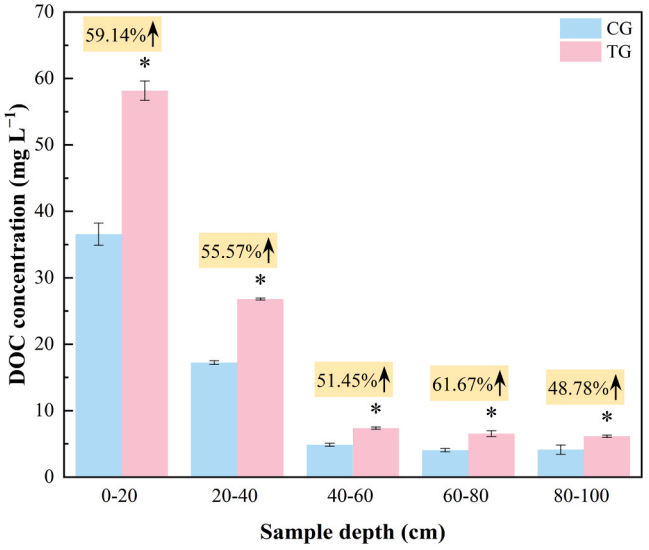


**Fig. 4.** Comparison of DOC concentration levels in the overlying water during the soil tillage experiment. CG represents control group, while TG represents tillage group. Values are presented as the average with standard deviation as error bars (AVG ± SD). Difference analysis was conducted by an independent-sample T-test (* represents $p < 0.05$ vs. CG at the same paddy soil interval).

leading to an increase of DOC concentration in paddy-field water by more than 55 %.

### 3.4. Variation of Hg in leachate sub-samples

#### 3.4.1. Effect of different Hg/DOC ratios

Average percentage rate of reduced Hg concentration (termed as $Hg_{reduction}$ rate) throughout the photoreduction experiment was calculated and plotted (Fig. 5). On Day 1, the 2 ng mL$^{-1}$ Hg solutions (Hg/DOC: 23–107 ng mg$^{-1}$) for different soil intervals showed the highest $Hg_{reduction}$ rates within the first 5 h, with 13.48 % h$^{-1}$, 5.53 % h$^{-1}$, 11.36 % h$^{-1}$, 7.75 % h$^{-1}$, and 4.41 % h$^{-1}$, respectively. Afterward, $Hg_{reduction}$ rate decreased sharply until sunset. The 5 ng mL$^{-1}$, 10 ng mL$^{-1}$ and 20 ng mL$^{-1}$ Hg solutions exhibited a similar pattern of $Hg_{reduction}$ rates to the 2 ng mL$^{-1}$ Hg solutions, but the $Hg_{reduction}$ rates tended to be decreased with the increase of Hg concentrations. On Day 2 and Day 3, $Hg_{reduction}$ rates of all solutions showed an overall increasing pattern, but the $Hg_{reduction}$ rates tended to be decreased with the increase of Hg concentrations.

After Hg(II) photoreduction, the fraction of Hg reduction (termed as $Hg_{reduction}$) was calculated (Fig. 6 and Text S4). The $Hg_{reduction}$ of the solutions was largely variable (9.02 ± 0.45 to 44.76 ± 2.24 %) and was closely associated with Hg/DOC ratio. At low Hg/DOC ratios, the $Hg_{reduction}$ in leachate of different soil intervals were much higher. For leachate from the same soil interval, the lower the concentration of exogenous Hg, the higher the photoreduction rate. When exogenous Hg was 2 ng mL$^{-1}$, Hg/DOC ratios varied from 23 to 107 ng mg$^{-1}$, and larger variation of $Hg_{reduction}$ (28.41 ± 1.42 to 44.76 ± 2.24 %) was observed in leachate, especially in leachate from surface soil interval (0–20 cm: 44.76 ± 2.24 %; 20–40 cm: 38.43 ± 1.92 %). As the

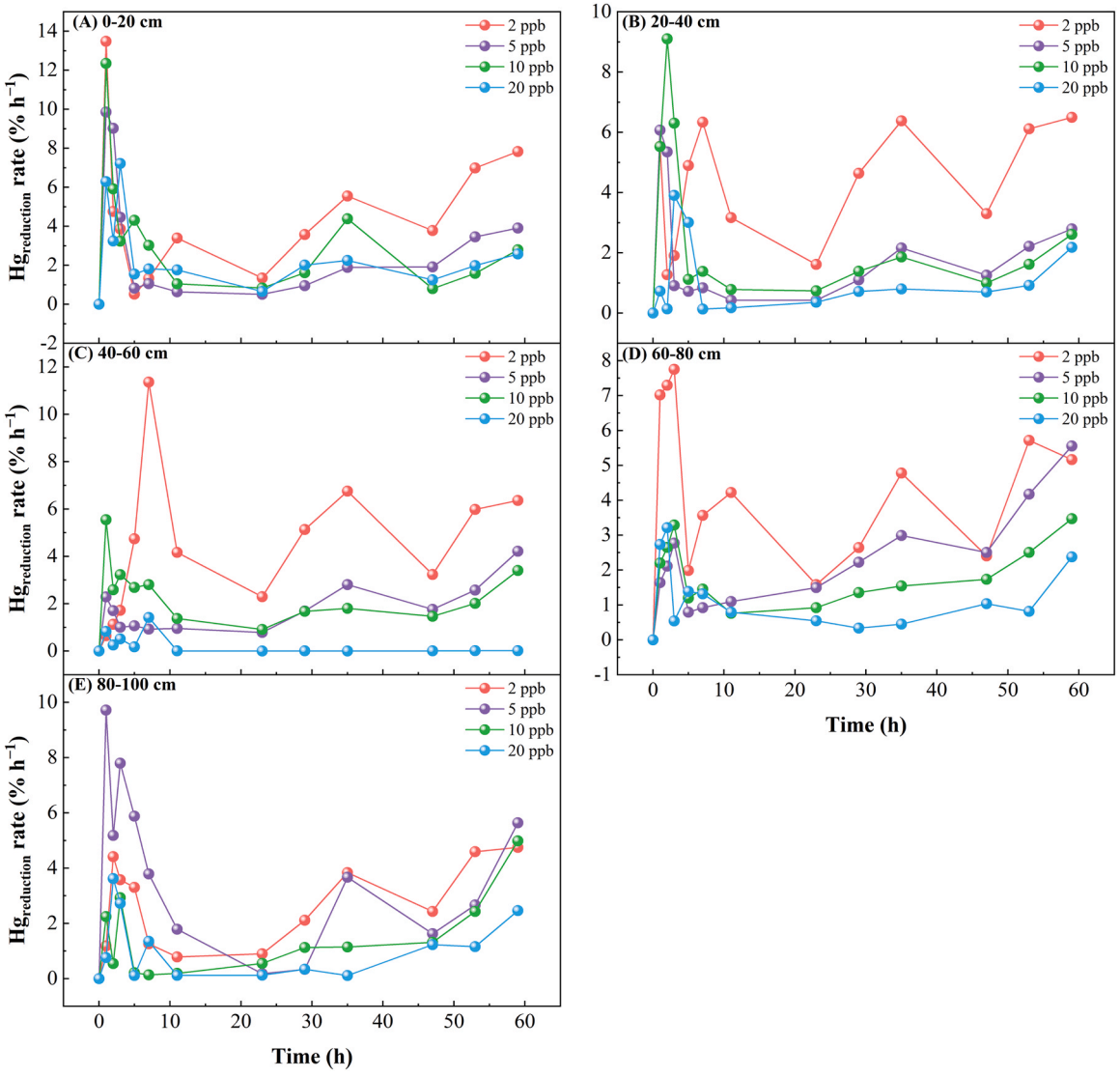


**Fig. 5.** Diurnal variation of $Hg_{reduction}$ rate: 0–20 cm (A), 20–40 cm (B), 40–60 cm (C), 60–80 cm (D) and 80–100 cm (E).

concentration of exogenous Hg increased, $Hg_{reduction}$ in leachate from different soil intervals showed a decreasing trend. When exogenous Hg reached 20 ng $mL^{-1}$, with Hg/DOC ratios ranging from 233 to 1066 ng $mg^{-1}$, $Hg_{reduction}$ of leachate from top to deep intervals decreased to 14.14 ± 0.71 %, 9.02 ± 0.45 %, 10.84 ± 0.54 %, 10.54 ± 0.53 % and 12.15 ± 0.61 %, respectively.

### 3.4.2. Role of solar radiation

The $Hg_{reduction}$ values decreased with the increase of Hg concentration, which appeared to be closely controlled by the amount of radiation absorbed by a single Hg atom (termed as $Radiation_{solar}/DOM_{mass}$) (Fig. 7). When $Radiation_{solar}/DOM_{mass}$ was the same, the $Hg_{reduction}$ of leachate from the same soil layer exhibited a decreasing trend as Hg/DOC ratios increases (0–20 cm: $Radiation_{solar}/DOM_{mass}$ was 0.03 mol m $g^{-1}$, $Hg_{reduction}$ decreased from 44.76 ± 2.24 to 14.14 ± 0.71 %; 20–40 cm: $Radiation_{solar}/DOM_{mass}$ was 0.08 mol m $g^{-1}$, $Hg_{reduction}$ declined from 38.43 ± 1.92 to 9.02 ± 0.45 %; 40–60 cm: $Radiation_{solar}/DOM_{mass}$ was 0.10 mol m $g^{-1}$, $Hg_{reduction}$ dropped from 37.63 ± 1.88 to 10.84 ± 0.54 %; 60–80 cm: $Radiation_{solar}/DOM_{mass}$ was 0.11 mol m $g^{-1}$, $Hg_{reduction}$ decreased from 31.39 ± 1.57 to 10.54 ± 0.53 %; 80–100 cm: $Radiation_{solar}/DOM_{mass}$ was 0.15 mol m $g^{-1}$, $Hg_{reduction}$ descended from 28.41 ± 1.42 to 12.15 ± 0.61 %). Thus, $Hg_{reduction}$ was closely related to solar radiation energy, and results in this study were partially consistent with the results of previous studies [13,24,50,51]. After exceeding the Hg/DOC ratio threshold, Hg(II) photoreduction was limited by solar radiation and decreased significantly with the increase of Hg/DOC ratio.

## 4. Discussion

### 4.1. Adsorption equilibrium time existed at the initial stage

Hg(II)-DOM complex is the primary form undergoing photoreduction [16,17]. At the initial stage of reaction, $SDOM_{0–20,20–40}$ tended to form weak complexes with Hg(II) (log*K* value was small) [9,52,53] due to their richer oxygen- and nitrogen-containing functional groups. By then, the weak binding pool predominated. As the reaction progressed, Hg(II)-SDOM complexes formed by strong bonding with thioalcohol (sulfur-containing functional groups) gradually occupied the dominant position [9,21,54]. However, the strong binding sites quickly reached saturation due to the low content of reduced sulfur in SDOM from different soil intervals, and subsequently, the weak binding sites predominated again [55,56]. This effectively revealed the existence of an "adsorption equilibrium time" between Hg(II) and SDOM during the initial stage of reaction (Day 1), which resulted in the occurrence of maximum $Hg_{reduction}$ rate (Fig. 5).

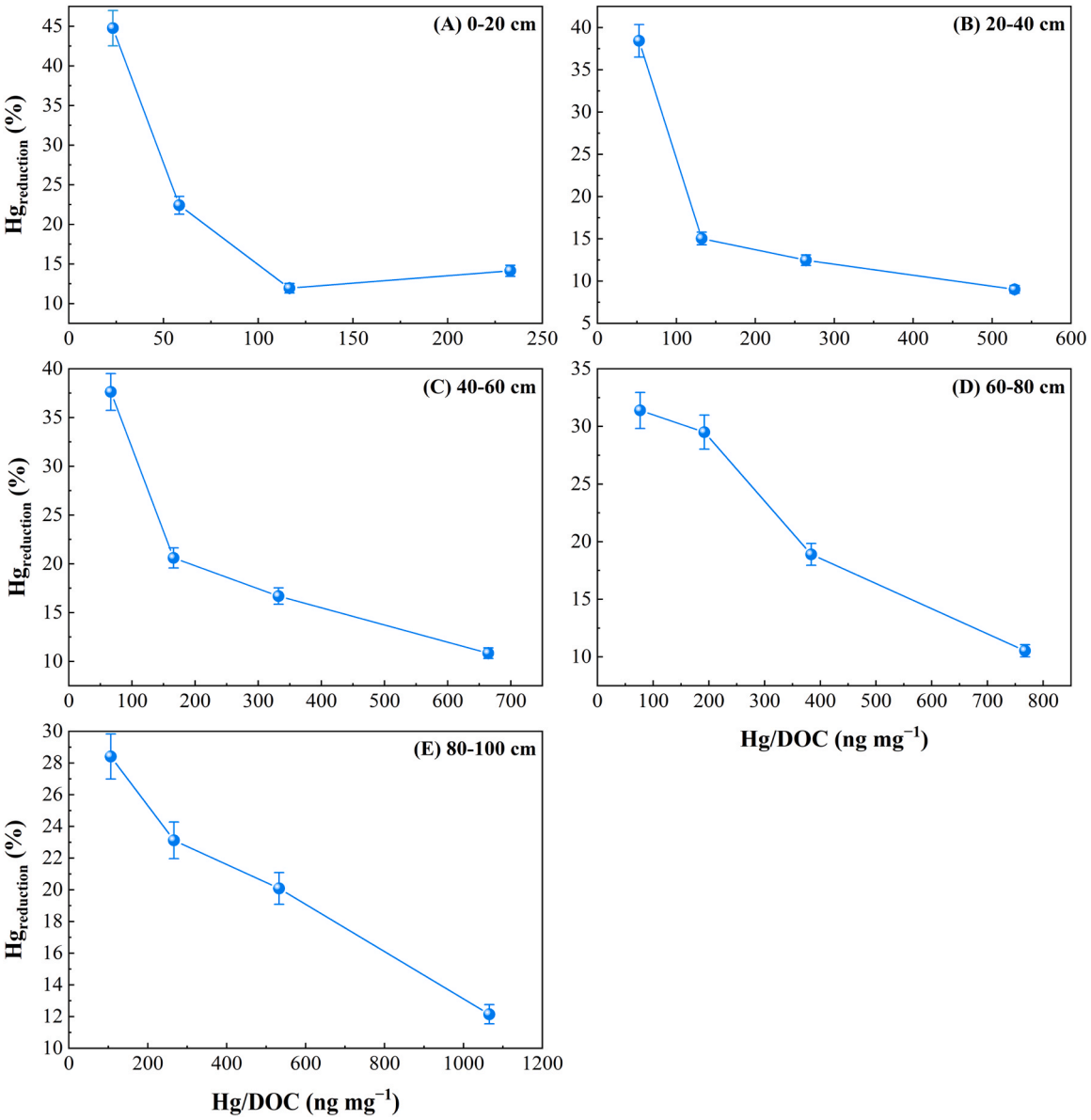


**Fig. 6.** Relationship between Hg/DOC ratio and $Hg_{reduction}$: 0–20 cm (A), 20–40 cm (B), 40–60 cm (C), 60–80 cm (D) and 80–100 cm (E). Values are presented as the average with standard deviation as error bars (AVG ± SD).

### *4.2. Solar radiation restricted photoreduction under high Hg/DOC ratio*

According to formula (1) [57], beakers containing leachate with varying Hg/DOC ratios were of equal size and positioned at the same place, which meant that the ε value per unit area for all beakers was the same. When the luminous flux density of each beaker was equal, and the combination degree and quantity of SDOM and Hg(II) would cause a great difference in the effective photon energy during the photoreduction process.

$$\varepsilon = hc/\lambda \quad (1)$$

where ε is photon energy; c is the speed of light; h is Planck constant; λ is the wavelength of light.

Hg had a high sensitivity to photons, and only after it absorbed enough photon energy could the electrons be excited [58], which led to a luminescence reduction reaction. In this study, a single SDOM in the leachate acted as an energy storage body that like a solar battery. As the reaction progressed (Day 2 and Day 3), SDOM continuously absorbed and stored light energy under sunlight. Therefore, at low Hg/DOC ratio, even when PAR weakened in the afternoon (Fig. S4), SDOM continued to provide the energy needed for Hg(II) photoreduction, thus $Hg_{reduction}$ rate continued to increase (Fig. 5). On the contrary, when at high Hg/DOC ratio, the sulfhydryl group (sulfur-containing functional group) as the primary site of Hg(II) binding (form strong Hg-SDOM complexes) [9,54–56] had reached the saturation state. The residual Hg(II) in the leachate complexed with oxygen- and nitrogen-containing functional groups through weakly bound (weak Hg-SDOM species) [24,52,59]. Less light energy SDOM received was redistributed to the multiple Hg atoms which complexed with. When the light energy transferred to a single Hg atom was not strong enough to cause the electronic excited state in weak Hg-SDOM species, stronger Hg-SDOM complexes were more unlikely to undergo photoreduction. For leachate from the same soil layer (with a certain SDOM concentration), light radiation energy distributed by DOM to a single Hg atom was significantly positively correlated with $Hg_{reduction}$ ($p < 0.02$) under high Hg concentration (Hg/DOC ratio) (Fig. 7). To sum up, the main limiting factor of Hg(II) photoreduction was solar radiation energy when Hg/DOC ratio was high.

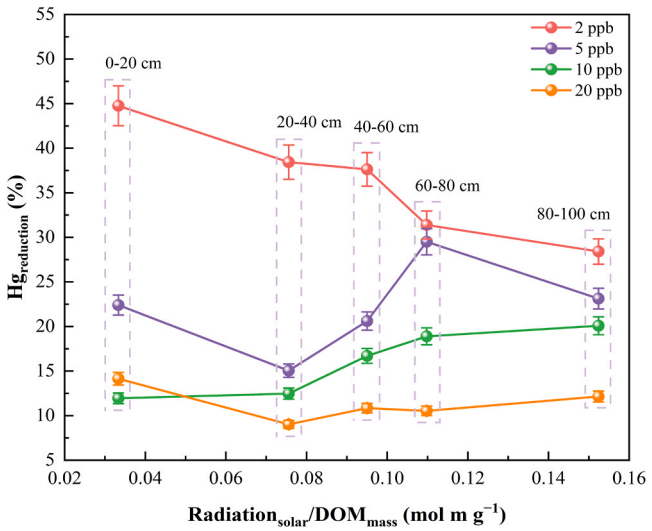


**Fig. 7.** Relationship between $Radiation_{solar}/DOM_{mass}$ and $Hg_{reduction}$. The dashed box represents leachate at the same paddy soil interval but with various Hg/DOC ratios. Values are presented as the average with standard deviation as error bars (AVG ± SD).

### 4.3. Surface SDOM facilitated photoreduction more efficiently under low Hg/DOC ratio

#### 4.3.1. Surface SDOM increased the mobility of Hg(II)

The pore and crack structure of $SDOM_{40–60,60–80,80–100}$ facilitated the diffusion of $Hg^{2+}$ into the interior of the SDOM molecule (Fig. 3-B). Once inside, $Hg^{2+}$ ions became trapped within the molecular network, making their escape difficult. Simultaneously, a significant portion of $Hg^{2+}$ formed stable covalent bonds with internal binding sites for complexation [60]. In this case, the binding between $SDOM_{40–60,60–80,80–100}$ and Hg(II) resulted in a reduced likelihood of desorption. The adsorption of $Hg^{2+}$ by $SDOM_{0–20,20–40}$ primarily occurred through the electrostatic action of functional groups on the surface of various spheres [61]. This type of bonding had relatively poor stability, allowing $Hg^{2+}$ to be released after desorption under certain conditions. Furthermore, due to the abundance of highly reactive oxygen- and nitrogen-containing functional groups, $SDOM_{0–20,20–40}$ showed a greater tendency to complex with Hg(II) [9,17,62]. This significantly increased the adsorption capacity of $SDOM_{0–20,20–40}$ for Hg(II), subsequently augmenting the solubility of Hg(II) in the liquid phase of the paddy field system [63]. Compared to $SDOM_{40–60,60–80,80–100}$, $SDOM_{0–20,20–40}$ served as a superior carrier for the migration and transformation of Hg(II). Therefore, the binding of $SDOM_{0–20,20–40}$ to Hg(II) played a pivotal role in facilitating efficient transport and widespread distribution of Hg(II) in paddy field system and adjacent aquatic environment.

#### 4.3.2. Surface SDOM reduced the stability of Hg(II)-SDOM complexes

Straw, as high-cellulose organic materials, were easy to be oxidized and degraded under aerobic conditions, providing a large amount of C and N sources for microbial activities [64]. Under the synergistic action of microbial-driven degradation and humification processes of relatively small molecular substances [65,66], the aromatic compounds within $SDOM_{0–20,20–40}$ accumulated rapidly, leading to an enhancement in the proportion of aromatic compounds with relatively complex structure (Fig. 2-A). The highly aromatic structure of $SDOM_{0–20,20–40}$ imparted it with a greater abundance of unsaturated conjugated bonds and other unstable structures. These features predisposed $SDOM_{0–20,20–40}$ to undergo free radical and cleavage reactions more readily, thereby diminishing the stability of Hg(II)-SDOM complexes [67].

Hydroxyl and carboxyl groups in DOM, as potential chelating centers of variable valence metal ions, are crucial functional groups influencing Hg(II) photoreduction [15,17,21]. The possible binding modes between carboxyl groups and $Hg^{2+}$ include unidetate, bindentate and bridging (Fig. S8). The binding constants for these modes are relatively low, making the bonds susceptible to cleavage [68]. $SDOM_{0–20,20–40}$ contained higher abundance of oxygen- and nitrogen-containing functional groups, which belong to weak binding sites for Hg(II) [9,24,53]. Meanwhile, the proportion of protein-like (C1) components in SDOM increased with the depth of soil interval (Fig. 2-B), and amino acids such as cysteine and leucine in protein components might serve as significant sources of thiols [69], thereby contributing to the augmentation of strong binding pool for Hg(II) [54,56]. Therefore, $SDOM_{0–20,20–40}$ tended to form a large number of structurally unstable Hg(II)-SDOM complexes, greatly enhancing the Hg(II) photoreduction.

#### 4.3.3. Surface SDOM enhanced generation of reactive intermediates

During the early and middle stages of photodegradation, photomineralization of DOM played a dominant role, which induce the production of transient reactive intermediates (RIs, e.g., $^3DOM^*$, $^1O_2$, $^{\bullet}OH$) (Fig. S9) [70,71]. By complexing Hg(II) under solar irradiation, DOM can generate RIs and highly active Hg(I) ($Hg_2^{2+}$ and $Hg^+$) species that are easily reduced (Eq. (2)) [19,24,71]. The high content of aromatic groups in $SDOM_{0–20,20–40}$ increases its photoreactivity, allowing it to absorb more light per unit of C [43]. Additionally, $SDOM_{0–20,20–40}$ contained a higher proportion of CDOM (such as hydroxyl, carboxyl, and carbonyl groups), which could undergo large-scale photodegradation. $SDOM_{0–20,20–40}$ could generate more RIs that mediate the Hg(II) photoreduction. This implies that, under the constraint of SDOM structure (at low Hg/DOC ratio), the amount of free radical generation played a decisive role in Hg(II) photoreduction. During the later stage of photodegradation, the complex internal structure of SDOM molecule was broken down, exposing more Hg(II) binding sites. Therefore, compared to $SDOM_{40–60,60–80,80–100}$, $SDOM_{0–20,20–40}$ was more conducive to Hg(II) photoreduction throughout the photodegradation process.

$$DOM\text{-}Hg^{2+} + hv \rightarrow RIs + Hg(I) \rightarrow Hg^0 \quad (2)$$

#### 4.3.4. Tillage synergistically enhanced photoreduction

Soil tillage can weaken the activity of soil microorganisms [72], leading to a reduction in the source of microbial metabolites in SDOM, which in turn decreases the degree of soil humification [65,66] and complexation strength between SDOM and heavy metals (like Hg) [72]. Undoubtedly, this process facilitates the Hg(II) photoreduction. Since soil tillage encompasses subsoil tillage and deep plowing, both of which are limited to the depth of 0–40 cm [29,49], this provides a plausible explanation for the relatively small difference in the degree of humification between $SDOM_{0–20,20–40}$ and $SDOM_{40–60,60–80,80–100}$ (Fig. 2-A). During the flooded period in the paddy system, tillage enhances soil porosity and the contact area between soil and water [73], accelerating the release of $SDOM_{0–20,20–40}$, which subsequently increases the amount of $SDOM_{0–20,20–40}$ in paddy-field water (Fig. 4). At the same time, soil tillage accelerates the infiltration of SDOM from various soil intervals into groundwater [74,75], eventually flowing into surface water. During the drainage period, $SDOM_{0–20,20–40}$ in paddy-field water can be transported into surrounding rivers via surface runoff. Wang et al. demonstrated that surface microrelief highly changed the partitioning of surface and sub-surface flow due to the tillage management, and DOM concentration in sub-surface flow was 7–18 times that in surface flow [74]. This indicates that soil tillage increases the input of SDOM (particularly $SDOM_{0–20,20–40}$) into paddy-field water and adjacent natural water, aqueous Hg(II) photoreduction tends to be greatly enhanced due to decreased Hg/DOC ratio.

### 4.4. Gear effect reduced Hg storage reservoir within paddy system

Based on the analysis of Section 4.3, the bond stability of Hg(II) with $SDOM_{0–20,20–40}$ was poorer than $SDOM_{40–60,60–80,80–100}$, yet $SDOM_{0–20,20–40}$ exhibited a higher adsorption capacity for Hg(II). This implies that less energy was required for Hg(II) photoreduction, leading to a more efficient process. Consequently, $SDOM_{0–20,20–40}$ could convert Hg(II) into Hg(0) more efficiently. During the non-flooded period in the paddy field system, solar radiation increased soil temperature, which accelerates both the thermal motion of soil Hg(0) and evaporation of soil moisture [76,77], thereby facilitating the diffusion process of Hg(0) through the soil-air interface. During the flooded period, soil matrices adsorbed by Hg(0) will desorb into the water phase, allowing Hg(0) to volatilize into the air [76]. Meanwhile, given that the stability of Hg (II)-DOM complex is significantly higher than that of heavy metal-soil/clay mineral complex [38], Hg(II) can more readily enter paddy-field water with SDOM. Soil, as the main force absorbing atmospheric Hg pollution [78], greatly reduces the adsorption capacity of paddy soil for Hg through the above process (Step 1: Reduction of Hg storage reservoir in paddy soil). The release of Hg(II) into paddy-field water subsequently undergoes photoreduction with SDOM and Hg(0) diffuses through the water-air interface (Step 2: Reduction of Hg storage reservoir in paddy-field water). Step 1 and Step 2 significantly reduce the Hg storage reservoir within paddy field system, thereby diminishing the source of MeHg and ultimately achieving the goal of mitigating MeHg accumulation in rice plants.

## 5. Conclusions and environmental implications

From paddy field systems to adjacent aquatic environments, the fate of Hg(II) was strongly influenced by its interaction with SDOM derived from different intervals of paddy soil. Hg(II) photoreduction mediated by SDOM was constrained by the structural composition of SDOM under low Hg/DOC ratios. Conversely, at high Hg/DOC ratios, the amount of solar radiation emerged as the dominant limiting factor. Straw returning and tillage jointly drove the transformation of $SDOM_{0–20,20–40}$ with higher aromaticity and richer oxygen-containing functional groups, while soil tillage increased the output of SDOM from paddy soil. The implementation of straw returning and soil tillage in managing paddy field system constitute a double-edged sword, which reduce Hg burden but increase the release flux of Hg(0). The latest findings by Zhang et al. [79] indicated that photoreduction obviously outweighed other Hg(II) reduction pathways within the paddy field system in terms of its contribution to Hg(0) emissions from paddy soil. This provided robust support for the reliability and significance of the experimental results obtained in this study. Given that the escape of Hg(0) caused by aqueous Hg(II) photoreduction is one of the main source for atmospheric Hg [8, 12,79]. This study further emphasizes the importance of this critical process for the global Hg cycle.

In various countries around the world, particularly in South and Southeast Asian where rice is a staple food, vigorously advocacy of paddy management measures (straw returning and soil tillage) will undoubtedly result in a huge release flux of Hg(0). Therefore, previous inventories of Hg(0) emissions from paddy field may have overlooked or underestimated the huge Hg(0) release flux caused by the gear effect of long-term straw returning and soil tillage. Furthermore, this study underscores the importance of considering the correlation between Hg(II)-SDOM binding pool and the characteristics of SDOM from different paddy soil intervals when assessing the mobility, bioavailability and potential ecological risks associated with Hg contamination in paddy soil environment. More importantly and meaningfully, this study also provides theory and empirical evidence for the fact that straw returning and soil tillage can effectively decrease the accumulation of MeHg in rice plants.

## Environmental implication

This study highlighted that straw returning and soil tillage were like a double-edged sword, with both advantages and disadvantages. Gear effect of straw returning and soil tillage significantly promoted aqueous Hg(II) photoreduction and reduced Hg burden in paddy field system, which could decrease the MeHg production and bioaccumulation in rice plants. However, previous inventories of Hg(0) emissions from paddy field may have overlooked or underestimated the huge Hg(0) release flux caused by the gear effect of long-term straw returning and soil tillage. Future global Hg cycling models should give special consideration to this process.

## Author contributions

The manuscript was written through contributions of all authors. All authors have given approval to the final version of the manuscript.

## CRediT authorship contribution statement

**Zhijun Fei:** Writing – review & editing, Writing – original draft, Visualization, Methodology, Investigation, Formal analysis, Data curation, Conceptualization. **Zhuhong Wang:** Writing – review & editing, Visualization, Validation, Resources, Methodology. **Jianxu Wang:** Writing – review & editing, Visualization, Formal analysis. **Shouyang He:** Writing – review & editing, Formal analysis. **Qixin Wu:** Writing – review & editing, Visualization, Validation, Supervision, Resources, Project administration, Funding acquisition. **Pan Wu:** Writing – review & editing, Visualization, Supervision.

## Declaration of Competing Interest

The authors declare that they have no known competing financial interests or personal relationships that could have appeared to influence the work reported in this paper.

## Acknowledgments

This work was supported by the National Natural Science Foundation of China (Nos. 42467032, 41603020), the Guizhou Science and Technology Project (QianKeHePingTaiRenCai-GCC[2023]061). The authors also greatly thank Researcher Runsheng Yin from Chinese Academy of Sciences, Prof. Wang Zheng from Tianjin University, and Dr. Jie Zeng from Guizhou University for their help in data analysis and discussion.

## Appendix A. Supporting information

Supplementary data associated with this article can be found in the online version at doi:10.1016/j.jhazmat.2024.136485.

## Data availability

Data will be made available on request.

## References

[1] Qin, C., Du, B., Yin, R., Meng, B., Fu, X., Li, P., et al., 2020. Isotopic fractionation and source appointment of methylmercury and inorganic mercury in a paddy ecosystem. Environ Sci Technol 54 (22), 14334–14342.
[2] Gustin, M.S., Bank, M.S., Bishop, K., Bowman, K., Branfireun, B., Chételat, J., et al., 2020. Mercury biogeochemical cycling: a synthesis of recent scientific advances. Sci Total Environ 737, 139619.
[3] Tokos, J.J.S., Hall, B., Calhoun, J.A., Prestbo, E.M., 1998. Homogeneous gas-phase reaction of $Hg^0$ with $H_2O_2$, $O_3$, $CH_3I$, and $(CH_3)_2S$: implications for atmospheric Hg cycling. Atmos Environ 32 (5), 823–827.
[4] Driscoll, C.T., Mason, R.P., Chan, H.M., Jacob, D.J., Pirrone, N., 2013. Mercury as a global pollutant: sources, pathways, and effects. Environ Sci Technol 47 (10), 4967–4983.

[5] Li, Y., Zhao, J., Zhong, H., Wang, Y., Li, H., Li, Y., et al., 2019. Understanding enhanced microbial MeHg production in mining-contaminated paddy soils under sulfate amendment: changes in Hg mobility or microbial methylators? Environ Sci Technol 53 (4), 1844–1852.
[6] Madenjian, C.P., Janssen, S.E., Lepak, R.F., Ogorek, J.M., Rosera, T.J., Dewild, J.F., et al., 2018. Mercury isotopes reveal an ontogenetic shift in habitat use by walleye in lower Green Bay of Lake Michigan. Environ Sci Technol Lett 6 (1), 8–13.
[7] Wang, K., Liu, G., Cai, Y., 2022. Possible pathways for mercury methylation in oxic marine waters. Crit Rev Environ Sci Technol 52 (22), 3997–4015.
[8] Bergquist, B.A., Blum, J.D., 2007. Mass-dependent and -independent fractionation of Hg isotopes by photoreduction in aquatic systems. Science 318 (5849), 417–420.
[9] Zheng, W., Hintelmann, H., 2009. Mercury isotope fractionation during photoreduction in natural water is controlled by its Hg/DOC ratio. Geochim Cosmochim Acta 73 (22), 6704–6715.
[10] Costa, M., Liss, P.S., 1999. Photoreduction of mercury in sea water and its possible implications for Hg0 air-sea fluxes. Mar Chem 68 (1-2), 87–95.
[11] Ravichandran, M., 2004. Interaction between mercury and dissolved organic matter-a review. Chemosphere 55 (3), 319–331.
[12] Bravo, A.G., Kothawala, D.N., Attermeyer, K., Tessier, E., Bodmer, P., Ledesma, J. L., et al., 2018. The interplay between total mercury, methylmercury and dissolved organic matter in fluvial systems: a latitudinal study across Europe. Water Res 144, 172–182.
[13] Wang, Z., Fei, Z., Wu, Q., Yin, R., 2020. Evaluation of the effects of Hg/DOC ratios on the reduction of Hg(II) in lake water. Chemosphere 253, 126634.
[14] Wang, Y., Liu, J., Liem-Nguyen, V., Tian, S., Zhang, S., Wang, D., et al., 2022. Binding strength of mercury (II) to different dissolved organic matter: the roles of DOM properties and sources. Sci Total Environ 807, 150979.
[15] O'Driscoll, N.J., Lean, D.R.S., Loseto, L.L., Carignan, R., Siciliano, S.D., 2004. Effect of dissolved organic carbon on the photoproduction of dissolved gaseous mercury in lakes: potential impacts of forestry. Environ Sci Technol 38 (9), 2664–2672.
[16] O'Driscoll, N.J., Siciliano, S.D., Lean, D.R.S., Amyot, M., 2006. Gross photoreduction kinetics of mercury in temperate freshwater lakes and rivers: application to a general model of DGM dynamics. Environ Sci Technol 40 (3), 837–843.
[17] O'Driscoll, N.J., Siciliano, S.D., Peak, D., Carignan, R., Lean, D.R.S., 2006. The influence of forestry activity on the structure of dissolved organic matter in lakes: implications for mercury photoreactions. Sci Total Environ 366 (2-3), 880–893.
[18] Gherini, S.A., Hudson, R.J.M., Watras, C.J., Porcella, D.B., 1994. Modeling the biogeochemical cycle of mercury in lakes: the mercury cycling model (MCM) and its application to the MTL study lakes. Mercury Pollut Integr Synth 473–522.
[19] Horvath, O., Vogler, A., 1998. Photoreduction of mercury(II) in aqueous solution in the presence of cyclohexene. Hydroxomercuration and two-stage photolysis. Inorg Chem Commun 1 (7), 270–272.
[20] Xiao, Z., Strömberg, D., Lindqvist, O., 1995. Influence of humic substances on photolysis of divalent mercury in aqueous solution. Water Air Soil Pollut 80, 789–798.
[21] Jeremiason, J.D., Portner, J.C., Aiken, G.R., Hiranaka, A.J., Dvorak, M.T., Tran, K. T., et al., 2015. Photoreduction of Hg(II) and photodemethylation of methylmercury: the key role of thiol sites on dissolved organic matter. Environ. Sci. Process. Imp. 17 (11), 1892–1903.
[22] Amyot, M., McQueen, D.J., Mierle, G., Lean, D.R.S., 1994. Sunlight-induced formation of dissolved gaseous mercury in lake waters. Environ Sci Technol 28 (13), 2366–2371.
[23] Tseng, C.M., Lamborg, C., Fitzgerald, W.F., Engstrom, D.R., 2004. Cycling of dissolved elemental mercury in Aritic Alaskan lakes. Geochim Cosmochim Acta 68 (6), 1173–1184.
[24] Gu, B., Bian, Y., Miller, C.L., Dong, W., Jiang, X., Liang, L., 2011. Mercury reduction and complexation by natural organic matter in anoxic environments. Proc Natl Acad Sci USA 108 (4), 1479–1483.
[25] Zhao, X., Li, R., Liu, W., Liu, W., Xue, Y., Sun, R., et al., 2024. Estimation of crop residue production and its contribution to carbon neutrality in China. Resour Conserv Recycl 203, 107450.
[26] Zhang, B., Dou, S., Guan, S., 2024. Enhancement of soil humic acid hydrophobicity by 5 consecutive years of full-amount straw shallow-mixed field return. Eur J Agron 161, 127378.
[27] Cheng, Z., Li, A., Wang, R., Hu, Q., Zhou, J., Li, M., et al., 2024. Long-term straw return promotes accumulation of stable soil dissolved organic matter by driving molecular-level activity and diversity. Agric Ecosyst Environ 374, 109155.
[28] Schmidt, M.P., Martínez, C.E., 2019. The influence of tillage on dissolved organic matter dynamics in a Mid-Atlantic agroecosystem. Geoderma 344, 63–73.
[29] Peng, Y., Chahal, I., Hooker, D.C., Van Eerd, L.L., 2024. Comparison of equivalent soil mass approaches to estimate soil organic carbon stocks under long-term tillage. Soil Res 238, 106021.
[30] Jiang, T., Kaal, J., Liang, J., Zhang, Y., Wei, S., Wang, D., et al., 2017. Composition of dissolved organic matter (DOM) from periodically submerged soils in the Three Gorges Reservoir areas as determined by elemental and optical analysis, infrared spectroscopy, pyrolysis-GC-MS and thermally assisted hydrolysis and methylation. Sci Total Environ 603-604, 461–471.
[31] Marschner, B., Kalbitz, K., 2003. Controls of bioavailability and biodegradability of dissolved organic matter in soils. Geoderma 113 (3/4), 211–235.
[32] Feng, X., Li, P., Qiu, G., Wang, S., Li, G., Shang, L., et al., 2008. Human exposure to methylmercury through rice intake in mercury mining Areas, Guizhou Province, China. Environ Sci Technol 42 (1), 326–332.
[33] Meng, B., Feng, X., Qiu, G., Cai, Y., Wang, D., Li, P., et al., 2010. Distribution patterns of inorganic mercury and methylmercury in tissues of rice (*Oryza sativa L.*) plants and possible bioaccumulation pathways. J Agric Food Chem 58 (8), 4951–4958.
[34] Tang, Z., Fan, F., Wang, X., Shi, X., Deng, S., Wang, D., 2018. Mercury in rice (*Oryza sativa L.*) and rice-paddy soils under long-term fertilizer and organic amendment. Ecotoxicol Environ Saf 150, 116–122.
[35] Ran, S., He, T., Zhou, X., Yin, D., 2022. Effects of fulvic acid and humic acid from different sources on Hg methylation in soil and accumulation in rice. J Environ Sci 119, 93–105.
[36] Abdelhafiz, M.A., Liu, J., Jiang, T., Pu, Q., Aslam, M.W., Zhang, K., et al., 2023. DOM influences Hg methylation in paddy soils across a Hg contamination gradient. Environ Pollut 322, 121237.
[37] Yang, X., Li, Z., Wang, T., Yang, Z., Wen, X., Yang, K., et al., 2023. Resupply, diffusion, and bioavailability of Hg in paddy soil-water environment with flood-drain-reflood and straw amendment. Environ Res 231, 116127.
[38] Zhou, L., Zhou, Y., Hu, Y., Cai, J., Bai, C., Shao, K., et al., 2017. Hydraulic connectivity and evaporation control the water quality and sources of chromophoric dissolved organic matter in Lake Bosten in arid northwest China. Chemosphere 188, 608–617.
[39] Selberg, A., Viik, M., Ehapalu, K., Tenno, T., 2011. Content and composition of natural organic matter in water of Lake Pitkjarv and mire feeding Kuke River (Estonia). J Hydrol 400 (1-2), 274–280.
[40] Huguet, A., Vacher, L., Relexans, S., Saubusse, S., Froidefond, J.M., Parlanti, E., 2009. Properties of fluorescent dissolved organic matter in the Gironde Estuary. Org Geochem 40 (6), 706–719.
[41] Ni, M., Li, S., 2019. Biodegradability of riverine dissolved organic carbon in a Dry-hot Valley Region: Initial trophic controls and variations in chemical composition. J Hydrol 574, 430–435.
[42] Hansen, A.M., Kraus, T.E.C., Pellerin, B.A., Fleck, J.A., Downing, B.D., Bergamaschi, B.A., 2016. Optical properties of dissolved organic matter (DOM): effects of biological and photolytic degradation. Limnol Oceanogr 61 (3), 1015–1032.
[43] McKnight, D.M., Boyer, E.W., Westerhoff, P.K., Doran, P.T., Kulbe, T., Andersen, D. T., 2001. Spectrofluorometric characterization of dissolved organic matter for indication of precursor organic material and aromaticity. Limnol Oceanogr 46 (1), 38–48.
[44] Yang, L., Chang, S.W., Shin, H.S., Hur, J., 2015. Tracking the evolution of stream DOM source during storm events using end member mixing analysis based on DOM quality. J Hydrol 523, 333–341.
[45] Taskin, E., de Castro Bueno, C., Allegretta, I., Terzano, R., Rosa, A.H., Loffredo, E., 2019. Multianalytical characterization of biochar and hydrochar produced from waste biomasses for environmental and agricultural applications. Chemosphere 233, 422–430.
[46] Abbas, Q., Yousaf, B., Ullah, H., Ali, M.U., Zia-ur-Rehman, M., Rizwan, M., et al., 2020. Biochar-induced immobilization and transformation of silver-nanoparticles affect growth, intracellular-radicles generation and nutrients assimilation by reducing oxidative stress in maize. J Hazard Mater 390, 121976.
[47] Wu, J., Wang, T., Zhang, Y., Pan, W., 2019. The distribution of Pb(II)/Cd(II) adsorption mechanisms on biochars from aqueous solution: considering the increased oxygen functional groups by HCl treatment. Bioresour Technol 291, 121859.
[48] Zhang, X., Li, Y., Ye, J., Chen, Z., Ren, D., Zhang, S., 2022. The spectral characteristics and cadmium complexation of soil dissolved organic matter in a wide range of forest lands. Environ Pollut 299, 118834.
[49] Wang, C., Yan, Z., Wang, Z., Batool, M., El-Badri, A.M., Bai, F., et al., 2021. Subsoil tillage promotes root and shoot growth of rapeseed in paddy fields and dryland in Yangtze River Basin soils. Eur J Agron 130, 126351.
[50] Amyot, M., Mierle, G., Lean, D., McQueen, D.J., 1997. Effect of solar radiation on the formation of dissolved gaseous mercury in temperate lakes. Geochim Cosmochim Acta 61 (5), 975–987.
[51] Rolfhus, K.R., Fitzgerald, W.F., 2001. The evasion and spatial/temporal distribution of mercury species in Long Island Sound, CT-NY. Geochim Cosmochim Acta 65 (3), 407–418.
[52] Drexel, R.T., Haitzer, M., Ryan, J.N., Aiken, G.R., Nagy, K., 2002. Mercury(II) sorption to two Florida Everglades peats: evidence for strong and weak binding and competition by dissolved organic matter released from the peat. Environ Sci Technol 36 (19), 4058–4064.
[53] Dong, W., Bian, Y., Liang, L., Gu, B., 2011. Binding constants of mercury and dissolved organic matter determined by a modified ion exchange technique. Environ Sci Technol 45 (8), 3576–3583.
[54] Song, Y., Jiang, T., Liem-Nguyen, V., Sparrman, T., Bjorn, E., Skyllberg, U., 2018. Thermodynamics of Hg (II) bonding to thiol groups in Suwannee River natural organic matter resolved by competitive ligand exchange, Hg LIII-edge EXAFS and $^{1}$H NMR spectroscopy. Environ Sci Technol 52 (15), 8292–8301.
[55] Hesterberg, D., Chou, J.W., Hutchison, K.J., Sayers, D.E., 2001. Bonding of Hg(II) to reduced organic sulfur in humic acid as affected by S/Hg ratio. Environ Sci Technol 35 (13), 2741–2745.
[56] Haitzer, M., Aiken, G.R., Ryan, J.N., 2002. Binding of mercury(II) to dissolved organic matter: the role of the mercury-to-DOM concentration ratio. Environ Sci Technol 36 (16), 3564–3570.
[57] Chen, Q., Chen, L., Qi, J., Tong, Y., Lv, Y., Xu, C., et al., 2019. Photocatalytic degradation of amoxicillin by carbon quantum dots modified $K_2Ti_6O_{13}$ nanotubes: effect of light wavelength. Chin Chem Lett 30 (6), 1214–1218.
[58] Meyer, T.J., 1986. Photochemistry of metal coordination complexes: metal to ligand charge transfer excited states. Pure Appl Chem 58 (9), 1193–1206.

[59] Yoon, S.J., Diener, L.M., Bloom, P.R., Nater, E.A., Bleam, W.F., 2005. X-ray absorption studies of $CH_3Hg^+$-binding sites in humic substances. Geochim Cosmochim Acta 69 (5), 1111–1121.
[60] Xu, D., Zhu, S., Chen, H., Li, F., 2006. Structural characterization of humic acids isolated from typical soils in China and their adsorption characteristics to phenanthrene. Colloid Surf A 276 (1-3), 1–7.
[61] Rashid, I., Murtaza, G., Dar, A.A., Wang, Z., 2020. The influence of humic and fulvic acids on Cd bioavailability to wheat cultivars grown on sewage irrigated Cd-contaminated soils. Ecotoxicol Environ Saf 205, 111347.
[62] Zhang, K., Gao, J., Men, D., Zhao, X., Wu, S., 2021. Insight into the heavy metal binding properties of dissolved organic matter in mine water affected by water-rock interaction of coal seam goaf. Chemosphere 265, 129134.
[63] Liu, X., Zhang, S., Wu, W., Liu, H., 2007. Metal sorption on soils as affected by the dissolved organic matter in sewage sludge and the relative calculation of sewage sludge application. J Hazard Mater 149 (2), 399–407.
[64] Chen, W., Westerhoff, P., Leenheer, J.A., Booksh, K., 2003. Fluorescence excitation-emission matrix regional integration to quantify spectra for dissolved organic matter. Environ Sci Technol 37 (24), 5701–5710.
[65] Leinweber, P., Schulten, H.R., Kalbitz, K., Meißner, R., Jancke, H., 2001. Fulvic acid composition in degraded fenlands. J Plant Nutr Soil Sc 164 (4), 371–379.
[66] Fang, Y., Nazaries, L., Singh, B.K., Singh, B.P., 2018. Microbial mechanisms of carbon priming effects revealed during the interaction of crop residue and nutrient inputs in contrasting soils. Glob Change Biol 24 (7), 2775–2790.
[67] Cornu, J.Y., Schneider, A., Jezequel, K., Denaix, L., 2011. Modelling the complexation of Cd in soil solution at different temperatures using the UV-absorbance of dissolved organic matter. Geoderma 162 (1-2), 65–70.
[68] Xia, Y., Yang, T., Zhu, N., Li, D., Chen, Z., Lang, Q., et al., 2019. Enhanced adsorption of Pb(II) onto modified hydrochar: modeling and mechanism analysis. Bioresour Technol 288, 121593.
[69] Wang, Z., Liao, J., Guo, X., Li, X., Kwon, S.Y., 2023. Total mercury in different egg tissues provides insights to mercury metabolisms in bird bodies. Ecotoxicol Environ Saf 249, 114336.
[70] Zeng, Y., Fang, G., Fu, Q., Dionysiou, D.D., Wang, X., Gao, J., et al., 2021. Photochemical characterization of paddy water during rice cultivation: formation of reactive intermediates for As(III) oxidation. Water Res 206, 117721.
[71] He, F., Zheng, W., Liang, L., Gu, B., 2012. Mercury photolytic transformation affected by low-molecular-weight natural organics in water. Sci Total Environ 416, 429–435.
[72] Ye, J., Perez, P.G., Zhang, R., Nielsen, S., Huang, D.F., Thomas, T., 2018. Effects of different C/N ratios on bacterial compositions and processes in an organically managed soil. Biol Fertil Soils 54 (1), 137–147.
[73] Blanco-Canqui, H., Gantzer, C.J., Anderson, S.H., Alberts, E.E., 2004. Tillage and crop influences on physical properties for an Epiaqualf. Soil Sci Soc Am J 68 (2), 567–576.
[74] Wang, H., Zhang, Q., Li, X., Yi, Y., Wang, Q., Gao, L., et al., 2023. Surface microrelief induced by tillage management alters the pathway and composition of dissolved organic matter exports from soils to runoff during rainfall. Water Res 245, 120554.
[75] Zeng, J., Han, G., Wu, Q., Qu, R., Ma, Q., Chen, J., et al., 2024. Significant influence of urban human activities and marine input on rainwater chemistry in a coastal large city, China. Water Res 257, 121657.
[76] Lin, C.J., Gustin, M.S., Singhasuk, P., Eckley, C., Miller, M., 2010. Empirical models for estimating mercury flux from soils. Environ Sci Technol 44, 8522–8528.
[77] Zhou, J., Wang, Z., Zhang, X., Driscoll, C.T., 2021. Measurement of the vertical distribution of gaseous elemental mercury concentration in soil pore air of subtropical and temperate forests. Environ Sci Technol 55, 2132–2142.
[78] Landis, J.D., Obrist, D., Zhou, J., Renshaw, C.E., McDowell, W.H., Nytch, C.J., et al., 2024. Quantifying soil accumulation of atmospheric mercury using fallout radionuclide chronometry. Nat Commun 15, 5430.
[79] Zhang, K., Pu, Q., Liu, J., Hao, Z., Zhang, L., Zhang, L., et al., 2024. Using mercury stable isotopes to quantify directional soil-atmosphere Hg(0) exchanges in rice paddy ecosystems: Implications for Hg(0) emissions to the atmosphere from land surfaces. Environ Sci Technol 58 (25), 11053–11062.